Location, Tilt, and Binding: A Molecular Dynamics Study of Voltage-Sensitive Dyes in Biomembranes

Marlon J. Hinner,*,† Siewert-J. Marrink, and Alex H. de Vries*

Groningen Biomolecular Sciences and Biotechnology Institute & Zernike Institute for Advanced Materials, Department of Biophysical Chemistry, University of Groningen, Nijenborgh 4, 9747 AG Groningen, The Netherlands

Received: August 18, 2009; Revised Manuscript Received: October 2, 2009

We present a molecular dynamics study on the interaction of styryl-type voltage-sensitive dyes with a lipid membrane. In this work, voltage-sensitive dyes are proposed as interesting model amphiphiles for biomolecular simulation, due to the wealth of biophysical and thermodynamical data available on their behavior and their binding to lipid membranes. Taking this data as a basis, we tested the recently developed MARTINI coarse-grained model (*J. Phys. Chem. B* **2007**, *111*, 7812). The focus was on the fast computation of the free energy of membrane binding. As a first step, we investigated the tilt and location of a coarse-grained representation of the dye Di-4-ASPBS in a lipid membrane, and found good agreement with atomistic simulations and experimental data. Then, we performed umbrella sampling to obtain the theoretical binding free energy for a number of Di-4-ASPBS derivates. In most cases, simulation and experimental binding data were in good agreement regarding the impact of structural changes in the amphiphile on binding. The work yields a general molecular picture of how such structural variations lead to changes of the binding mode and binding strength of amphiphiles to lipid membranes. Further, it provides insights into the possibilities and current limitations of rapid free energy computation for membrane binding with the coarse-grained MARTINI model. The results suggest that the MARTINI model may be a generally useful tool for the study and optimization of molecules interacting with membranes, such as biophysical probes or pharmaceutical compounds.

Introduction

Voltage-sensitive hemicyanine dyes are fluorescent probes for monitoring the electrical activity of nerve cells.[1−3] The dyes are amphiphilic and bind to membranes, where they report changes in transmembrane potential by a change in their fluorescence with submillisecond time resolution. Prominent examples of these compounds,[2,4−6] which are synonymously also called "styryl-type" dyes due to their shared basic structure, are depicted in Figure 1. The sensitivity of the dyes to electric field changes has made them valuable probes also for other applications, such as the study of membrane dipole potential[7] or of the reaction mechanism of ion pumps, for example, the Na^+,K^+-ATPase.[8] Further, styryl-type dyes such as FM 1-43 are important for staining membranes in general due to their favorable fluorescent properties and adjustable lipophilicity. A particularly important application is the study of vesicle trafficking, for example, in actively firing neurons.[9−11]

Voltage-sensitive dyes have been the subject of intense biophysical study, aimed at understanding their interaction with biomembranes and the mechanism by which their fluorescence is affected by a change in transmembrane potential.[2,5,12−21] In particular, the binding of various derivates of these dyes to lipid membranes has been studied in detail.[2,12−17] Because the fluorescence quantum yield of many of the dyes is enhanced upon binding to lipid membranes, their partition coefficients between water and the lipid phase can be determined with high accuracy by fluorescence lipid titration.[12] Binding studies using voltage-sensitive dyes have provided interesting insights into how structural changes affect their binding free energies. For example, one study investigated the impact of the alkyl chain length at the hydrophobic tail of the amphiphilic dyes on the free energy of binding, and found a linear increase with increasing chain length.[12] In more recent work, hydroxyl and phosphoric acid ester groups were introduced into the dye structure and their impact on binding was determined.[13−15] These studies led to the development of voltage-sensitive dyes that can be induced to bind to lipid and cell membranes by enzymatic removal of the phosphoric acid ester group (Figure 2).[13−15]

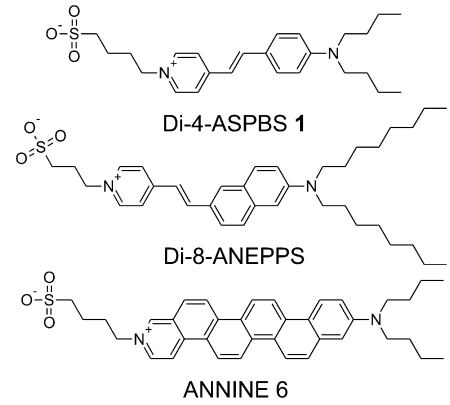

Figure 1. Examples for styryl-type voltage-sensitive dyes.

We wanted to investigate whether computational tools could be used to explain and predict the binding of amphiphilic molecules such as the voltage-sensitive dyes to lipid membranes, using the available experimental data as a reference. Molecular

* To whom correspondence should be addressed. E-mail: marlon.hinner@epfl.ch (M.J.H.); a.h.de.vries@rug.nl (A.H.d.V.).

† Current Address: Institute of Chemical Sciences and Engineering, Laboratory of Protein Engineering, École Polytechnique Fédérale de Lausanne, CH-1015 Lausanne, Switzerland.

10.1021/jp907981y CCC: $40.75
Published on Web 11/06/2009

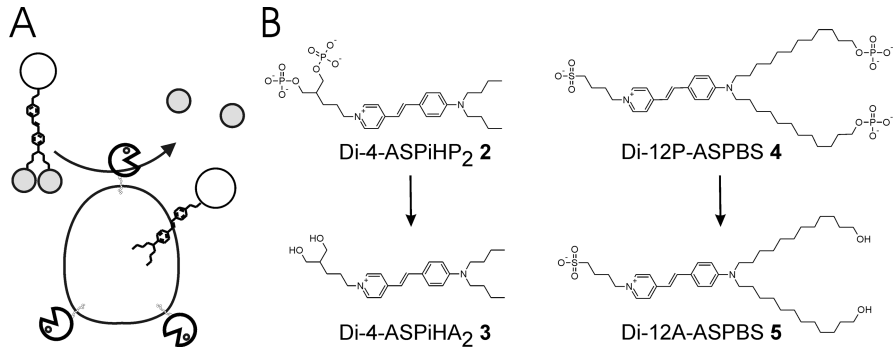

Figure 2. Concept of enzyme induced staining and voltage-sensitive dyes used therein. (A) Concept. An amphiphilic voltage-sensitive dye (polar headgroup indicated by white circle) is derivatized with enzymatically cleavable polar groups (represented by gray circles). An ectoenzyme is expressed on the surface of a cell. Hydrolysis of the precursor dye by the enzyme produces a dye that binds to the cell membrane. (B) Dyes. Model precursor dyes used in enzyme activated binding are derivates of Di-4-ASPBS (**1**). They contain phosphate groups at the head (dye **2**) or tail (dye **4**) which confer water solubility and impair binding to a biomembrane. By enzymatic hydrolysis, the corresponding, more strongly binding dyes **3** and **5** are formed.

dynamics (MD) simulations seemed promising for this task, because they have been increasingly and successfully applied during the last years to study the interaction of small molecules with lipid membranes.[22] Until recently, however, using MD simulations to estimate the partition coefficients for molecules containing more than a few atoms was not feasible, as binding and unbinding events occur at a time scale not easily sampled in MD simulations. Using methods to facilitate sampling, estimates of the free energy of binding of a range of molecules of limited size, including water,[23] hexane,[24] and other small penetrants have been obtained.[25−27] In very recent state of the art simulations, partition coefficients and flip-flop rates for complex compounds with multiple internal degrees of freedom, such as amino acids[28] or lipids,[29−31] have successfully been computed. Still, the computational cost of obtaining the binding free energy to membranes is enormous, in particular for large molecules. This makes systematic studies on a large number of compounds impractical. We therefore turned our attention to computationally less costly simulation methods that employ coarse-grained models.[32−34] In coarse-graining, molecules are represented in a simplified way, with multiple atoms being combined into one interaction site, also called a bead. While this leads to a loss of atomistic resolution of the system, it allows speeding up simulations by orders of magnitude while many properties of the system are semiquantitatively preserved.

In this publication, we apply coarse-grained molecular dynamics simulations to obtain estimates of the membrane binding free energy of the voltage-sensitive dye Di-4-ASPBS (**1**) (dibutyl-amino-styryl-pyridinium-butyl-sulfonate, Figure 1) and its derivates with varying alkyl chain length and additional polar groups (Figure 2B). The study also provides molecular insights into the behavior of such dyes in lipid membranes. First, we describe the construction of a coarse-grained model of Di-4-ASPBS (**1**) within the framework of the recently developed MARTINI 2.0 force field.[35] The overall flexibility of bonds, angles, and dihedrals is adapted to an atomistic model of the same dye which was constructed using the GROMOS 53A6 force field.[36] Then, the coarse-grained model is validated by comparing its location and orientation in a lipid membrane to the atomistic model and to experimental data of structurally related styryl-type dyes. Finally, umbrella sampling simulations[37] are carried out to obtain the potentials of mean force (PMF) in a lipid membrane for Di-4-ASPBS (**1**) and its derivatives. Particular attention is paid to finding the proper conditions for umbrella sampling that guarantee convergence of PMF profiles irrespective of the starting configuration. From the potentials of mean force, we compute free energies of binding ΔG_{PMF}, and compare them to experimental free energies of binding ΔG_{EXP} obtained from appropriately converted experimental binding constants.

Materials and Methods

Atomistic Molecular Dynamics Simulations. Atomistic level simulations were performed using the GROMACS 3.3.1 package[38,39] using force field parameters compatible with the GROMOS 53A6 force field.[36] An atomistic, united-atom model of the dye Di-4-ASPBS (**1**) in accordance with GROMOS building blocks was constructed.[40] The charge distribution in this model was obtained by performing dipole preserving charge (DPC) analysis[41] of the quantum chemical charge distribution using the GAMESS-UK software package.[42] DPC analysis yields point charges that optimally preserve overall and local dipole moments of the quantum-chemical charge distribution. For the lipid POPC, a modified parameter set was used.[43] Details of the dye and POPC topologies and parameters are given in the Supporting Information. The simple point charge (SPC) model of Berendsen et al. was used to model water.[44]

A Berendsen thermostat[49] was used with a coupling constant of 0.1 ps in all simulations, and the reference temperature was set to 323 K in all simulations. In membrane simulations, pressure coupling was applied semiisotropically, coupling the pressure tensor in the directions parallel to the membrane surface separately from the direction perpendicular to the membrane surface, also using the Berendsen scheme with a coupling constant of 0.5 ps. The reference pressure was 1 bar in all directions, and the compressibility was 4.6×10^{-5} bar^{-1}. The box shape was rectangular, and periodic boundary conditions were applied to all systems. Bond lengths were constrained with the LINCS algorithm.[45] The water geometry was constrained using the SETTLE algorithm.[46] A time step of 2.0−2.5 fs was used.

Nonbonded interactions were calculated using a twin-range cutoff scheme.[47] They were truncated at a distance of 1.4 nm, updated every time step in the range 0.0−0.9 nm, and every five steps in the range 0.9−1.4 nm. A reaction field correction[48] was applied to alleviate straight-cutoff Coulomb artifacts, using a dielectric permittivity of 54, appropriate for the SPC water model. Two simulations were performed: (i) Di-4-ASPBS (**1**) (41 atoms) with 3317 SPC water molecules (50 ns at 2.0 fs time step) and (ii) Di-4-ASPBS (**1**) in a membrane of 64 POPC molecules in a bilayer and 1586 SPC water molecules (45 ns at

2.5 fs time step). Coordinates and velocities were written every 10 000 steps.

Coarse-Grained Molecular Dynamics Simulations. Coarse-grained molecular dynamics simulations were performed with the GROMACS[38,39] software package, version 3.3.1, and the MARTINI forcefield, version 2.0.[35] For production runs, a time step of 40 fs was used in all simulations. The temperature and pressure (1 bar) were kept constant by using a weak-coupling algorithm[49] (Berendsen coupling) with relaxation times of 0.5 and 1.2 ps, respectively. For sytems containing a membrane, the water (including ions) and membrane components (including the molecule of interest) were thermostatted separately. In membrane simulations, we applied semiisotropic pressure coupling using 1 bar in z and lateral directions; otherwise, pressure coupling was performed isotropically. The box shape was rectangular, and periodic boundary conditions were applied to all systems. Apart from the free energy calculations described below in detail, the following systems were simulated with Di-4-ASPBS (**1**), using two different topologies for the molecule and a timestep of 40 fs (cf. Results): (i) Di-4-ASPBS (**1**) in a box of 1717 MARTINI water molecules at 323 K at an overall simulation time of 50 ns, with writing out coordinates and velocities every five steps. (ii) Di-4-ASPBS (**1**) in a bilayer of 128 POPC lipid molecules containing 1483 MARTINI water particles at 323 K (380 ns). Note that the sampling times indicated are not scaled to the effectively sampled time, which would be 4 times longer; this increase in the speed of dynamics in coarse-grained simulations is due to a smoothened energy landscape.[35,50] Coordinates and velocities were written every 1000 steps (40 ps).

Coarse-Grained Model Building. To construct a coarse-grained model of Di-4-ASPBS (**1**) (Figure 3 depicts the final model), we started by following the published standard recipe,[35] i.e., (i) groups of around four atoms which were not part of a ring formed one bead. This related to the butyl residues in the tail and the headgroup, as well as for the sulfonate headgroup. (ii) Each aromatic ring was constructed by three beads belonging to a special ring-type bead class to form a benzene-like ring. The benzene ring geometry was adapted to allow for the *para*-disubstitution of both rings, as indicated in Figure 3. (iii) Charges were assigned to single beads, i.e., a charge of −1 to the sulfonate headgroup and a charge of +1 to the pyridinium amine. To account for the polarity of the latter, it was assigned a more polar particle type than the normal C1 ring type.

This left some nonstandard problems in topology construction; the final choices were made according to practical considerations and to allow a large 40 fs time step in the simulations. We decided to (iv) disregard the double bond in the chromophore and directly connect the two aromatic rings with a bond that reflected the actual distance in the molecule; (v) explicitly keep the aniline nitrogen atom as a branching point; and (vi) ensure the overall planarity of the aromatic ring system by introducing a number of improper dihedrals in analogy to the procedure used in atomistic model building.[21] The use of proper dihedrals to control the relative movement of planes of the aromatic rings with respect to each other (the twisting movement) and to keep the beads that are directly attached to the chromophore (beads 2 and 9 in Figure 3) within the same plane was not compatible with large time steps. The same was observed when we tried to introduce a barrier against rotation of the aniline C−N bond which has partial double-bond character. Therefore, we decided to control the twisting movement by introducing two extra bonds between beads 5 and 7 as well as between beads 4 and 6, while allowing the aniline C−N bond to rotate freely. The coarse-grained topology of the dye that was obtained in this first attempt was constructed using standard values for the angles and force constants, except for (i) the bonds between atom pairs 5−6, 5−7, and 4−6, which were tentatively assigned a value of 5000 kJ mol^{-1} nm^{-2}, (ii) the bond between atoms 8 and 9, which was shortened to 0.37 nm to reflect the fact that bead 9 only represents one atom, (iii) the improper dihedrals, which were tentatively assigned a force constant of 50 kJ mol^{-1} rad^{-2}, and (iv) the angles describing the relative geometry between the two aromatic rings, which were adapted to reflect the actual geometry of the aromatic system.

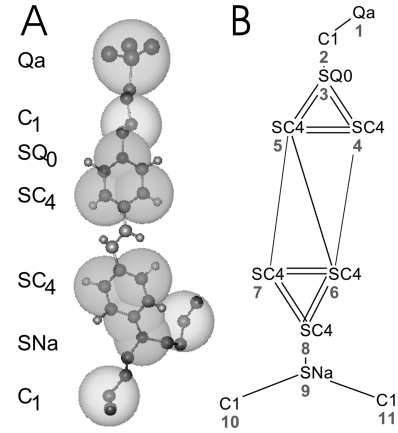

Figure 3. Coarse-grained model of the voltage-sensitive dye Di-4-ASPBS (**1**). (A) Ball-and-stick model of Di-4-ASPBS (**1**) (solid) with transparent spheres indicating the mapping of the chemical structure onto a coarse-grained representation. The corresponding bead types are indicated on the left. (B) Coarse-grained representation of Di-4-ASPBS (**1**) showing bead types, their numbering, and the bonds between them. The standard values of length l and force F are $l = 0.47$ nm and $F = 1250$ kJ mol^{-1} nm^{-2} for a single bond and $l = 0.27$ nm for a constraint (shown as a double bond). For angles, the standard value was assigned according to geometric considerations, and the standard force constant was $K_{angle} = 25.0$ kJ mol^{-1}. The Qa and SQ0 beads were assigned a charge of –1 and +1, respectively. The following nonstandard values were assigned: *bonds* (atom1−atom2 length force_constant [kJ mol^{-1} nm^{-2}]) 5−6 0.59 5000; 8−9 0.37 2500; 4−6 0.55 1250; 5−7 0.55 1250. *angles* (atom1−atom2−atom3 angle force [kJ mol^{-1}]) 3−5−6 135 200; 4−5−6 75 250; 5−6−7 75 250; 5−6−8 135 200; 8−9−10 120 60; 8−9−11 120 60; 10−9−11 120 60; 7−8−9 150 250; 6−8−9 150 250. *improper dihedrals* (atom1−atom2−atom3−atom4 angle force [kJ mol^{-1} rad^{-2}]) 4−5−7−6 0.0 25; 3−5−8−6 0.0 25; 4−7−8−6 0.0 25; 6−5−3−4 0.0 25. *exclusions* (between all atoms) 4 6 7 8; 3 6 7 8; 5 6 7 8.

The basic dye model was optimized by comparing distributions of angles and dihedrals in the coarse-grained model in free simulations to those in a mapped atomistic model of Di-4-ASPBS (**1**) (Supporting Information). For mapping the atomistic trajectory onto the coarse-grained topology, the program *g_traj* which is part of the GROMACS software package was modified to allow writing the centers of mass of indexed groups to be written into xtc format. The mapping was performed as indicated in Figure 3, except for the beads corresponding to the aromatic rings, where single atoms were mapped onto the corresponding beads in order to allow for the correct geometry. Tables with the resulting fitted parameter values for selected angle and dihedral potentials of the atomistic model and the coarse-grained models can be found in the Supporting Information. Comparing the coarse-grained starting structure to the mapped atomistic model, we found that all average angles were in good agreement with each other in both models. However, the angles involving the aniline nitrogen (bead 9 in Figure 3) and the angles between the beads in the

chromophore were too flexible in the coarse-grained model, and the out-of-plane movements of the beads attached to the aromatic rings did not agree with the atomistic simulation.

Iteratively, a new topology of the dye was constructed with reduced bond and dihedral force constants in the chromophore, which improved the agreement with the atomistic model regarding the out-of-plane movement, and angle force constants were increased where necessary. The force constants used in the final model are given in the caption of Figure 3. The overall flexibility of the final coarse-grained model was in good accord with the mapped atomistic model, except for the fact that it exhibited no barrier to rotation in the dialkylamine moiety, and that the stiffness of the chromophore with regard to a twisting movement was too high. Since it is not expected that these deviations strongly affect the properties of interest, i.e., the binding position and tilt angle in the membrane and the PMF profiles, the model was used as such.

The models for the other molecules used in the simulations, which are all derivatives of Di-4-ASPBS (**1**), were constructed on the basis of the Di-4-ASPBS (**1**) model according to the standard recipe unless stated otherwise. The models are described in the Results and Discussion section.

Computation of the Potential of Mean Force. The potential of mean force (PMF) was calculated using umbrella sampling.[37] The systems used consisted of the molecule of interest, 128 POPC molecules in a bilayer membrane, and up to 1500 coarse-grained waters ("small system") or up to 3373 coarse-grained waters ("large system"), respectively. For charged compounds, coarse-grained sodium or chloride ion particles were included in the system to ensure overall neutrality. The systems were generated from a box containing the membrane and coarse-grained waters by replacing the necessary number of water molecules by the molecule of interest and countercharges, subsequent energy minimization (1000 steps using the steepest descent method), and a run of 10 ns at a time step of 40 fs. The latter was performed to ensure equilibration and to check whether the system was numerically stable under these conditions. The simulations were carried out at 323 K. Starting from a position where the molecule of interest is at its equilibrium position in the membrane, the molecules were forced to approach their umbrella sampling position for 200 ps with a time step of 1 fs and a force of 500 kJ mol^{-1} nm^{-2}. The umbrella potential was applied to one or two beads which were close to the center of the molecule (cf. Results and Discussion). The spacing between umbrella positions was 0.1 nm, and umbrella positions evenly covered the distance from the water phase to the membrane center. Depending on the molecule under study, the covered distance was from −4.7 or −4.1 nm to 0.2 nm from the membrane center. Here, the small system was employed for umbrella positions −1.5 to 0.2 nm, while the large system covered −4.7 to −1.5 nm, with one overlapping position that allowed validating that the potential of mean force at this position was the same for both systems. After initialization, the umbrella potential was increased to 5000 kJ mol^{-1} nm^{-2}, and the simulation was run for a total of 100 ns. The potential of mean force profile was constructed from the biased distributions of the centers of mass of the molecule of interest using the weighted histogram analysis method[51] with a relative tolerance of 10^{-6}. The script used for this purpose was a kind gift from the Tieleman group. The PMF profiles were computed separately from 0 to 20 ns (the equilibration phase) and from 20 to 60 ns and 60 to 100 ns (the production phase), respectively. This approach allowed an insight into which parts of the profile were most subject to change within the first 20 ns of the simulation. Comparing the results for the first half and the second half of the production phase allowed assessing the variability associated with the obtained free energy profiles. Selected umbrella positions of the large system (cf. Results) were continued to run to a total of 500 ns. The final PMF profiles were again constructed with the full trajectory, and the respective first and second half of each trajectory.

Relationship between Experimental Binding Constants and Potential of Mean Force. The potential of mean force we calculate is the free energy associated with moving the dye molecule from a reference position along the z-axis to a particular position along the z-axis. The PMF is connected to the probability profile $p_D(z)$ for the dye being at a position along the z-axis via the Boltzmann relation, with molar gas constant R and temperature T:

$$p_D(z) = \exp[-\Delta\mathrm{PMF}(z)/RT] \tag{1}$$

ΔPMF is the value of the PMF (in J mol^{-1}) relative to the reference point, which we choose to be the mimimum of our computed PMF. In the PMF profiles obtained in the present study (cf. Figures 8−11), this minimum is located at a position within the membrane. Note that the PMF profile of a compound in a symmetric lipid membrane is symmetric; therefore, we have only computed the PMF for one leaflet of the membrane. A partition coefficient of the dye between the membrane and the water phase can be obtained straightforwardly from the relative probability profile by integrating along the z-axis over the appropriate regions defining membrane-bound and membrane-unbound dye. Choosing the center of the bilayer as the origin of the z-axis, integrating over one leaflet of the bilayer up to a distance Z_M from the center, and multiplying by 2 to account for the other leaflet of the membrane, the total relative membrane-bound probability P_M is given by eq 2:

$$P_M = 2\int_0^{Z_M} \mathrm{d}z\, p_D(z) \tag{2}$$

To allow a comparison of experimental data with the computed PMFs, we now define a dimensionless partition coefficient $C_{Mem/Wat}$ by relating the total relative probability of membrane-bound dye P_M divided by the length of the region defined as the membrane $2 \times Z_M$ to the probability of finding the dye in the membrane-unbound or water phase p_D^W:

$$C_{Mem/Wat} = \frac{P_M/2Z_M}{p_D^W} = \frac{\int_0^{Z_M} \mathrm{d}z\, p_D(z)}{p_D^W Z_M} \tag{3}$$

Note that we choose our Z_M such that a plateau value has been reached in the relative probability profile and that the relative probability of the membrane-unbound dye (or dye in the water phase) p_D^W is the same everywhere in the nonmembrane phase. The free energy of transfer from water to the membrane that is associated with $C_{Mem/Wat}$ can then be calculated by eq 4:

$$\Delta G_{PMF} = -RT \ln C_{Mem/Wat} = -RT \ln \frac{\int_0^{Z_M} \mathrm{d}z\, p_D(z)}{p_D^W Z_M} \tag{4}$$

The value obtained is slightly less negative than the difference between the values of the PMF in water and at its minimum position, reflecting the fact that the probability profile is not constant over the entire region defined as the membrane.

Experimental binding constants K_{EXP} of compounds such as the voltage-sensitive fluorescent dyes are usually obtained in terms of the concentration of membrane-bound dye c_M, con-

centration of membrane-unbound dye c_W, and concentration of lipid c_L according to eq 5:[12,13]

$$K_{EXP} = \frac{c_M}{c_W c_L} \quad (5)$$

In order to compare partition coefficients derived from experimental and PMF data, respectively, the partition coefficients must be put on equal par by considering how the system that was used to obtain the PMF relates to the system that was used to define the experimental binding constants. Note that, in eq 5, c_W was defined as the concentration of dye in the volume of water only (i.e., excluding the membrane volume) but that c_M measures the concentration of dye in the membrane relative to the total volume of the system. Our computational setup consists of a rectangular volume with area A_L, so that $V_T = A_L Z_T$ is the total volume and $V_L = 2Z_M A_L$ is the volume of the membrane. Z_T is the length defining the total volume considered, and A_L is also the area of the lipid membrane phase which is modeled as a lamellar bilayer consisting of N_L lipids per bilayer. Thus, in our setup, K_{EXP} can be written as

$$K_{EXP} = c_M \frac{1}{c_W}\frac{1}{c_L} = \frac{2\int_0^{Z_M} dz\, p_D(z) A_L}{V_T} \frac{(V_T - V_L)}{\int_{2Z_M}^{Z_T} dz\, p_D^W A_L} \frac{V_T}{N_L} = \frac{2\int_0^{Z_M} dz\, p_D(z)}{p_D^W} \frac{A_L (Z_T - 2Z_M)}{(Z_T - 2Z_M)} \frac{1}{N_L} = \frac{P_M}{p_D^W}\frac{A_L}{N_L} \quad (6)$$

Comparing to eq 3, and converting to appropriate molar units, with a_L being the area per lipid and N_{Av} Avogadro's number, we arrive at eq 7:

$$K_{EXP} = \frac{c_M}{c_W c_L} = \frac{P_M}{p_D^W}\frac{A_L}{N_L} = C_{Mem/Wat} Z_M a_L N_{Av} \quad (7)$$

Using typical values of $Z_M = 2$ nm (corresponding to the thickness of one leaflet of a membrane) and $a_L = 0.64$ nm^2/molecule, we obtain a conversion factor of $Z_M a_L N_{Av} = 2 \times 0.64 \times 10^{-24} \times 6.023 \times 10^{23} = 0.77$ L mol^{-1}. With this relation, we can compute a free energy of transfer ΔG_{EXP} which can be directly compared to ΔG_{PMF} by eq 8:

$$\Delta G_{EXP} = -RT \ln(K_{EXP}/Z_M a_L N_{Av}) = -RT \ln(K_{EXP}/0.77\ \text{L mol}^{-1}) \quad (8)$$

Equation 8 is equivalent to a relation derived by Fromherz and Röcker.[12] For the interconversion of partition coefficients corresponding to different units, see the publication by Lasch.[52]

Results and Discussion

Construction of the Model. As the starting point for simulations, a coarse-grained model of Di-4-ASPBS (**1**) was constructed. Di-4-ASPBS (**1**) is the parent compound for all voltage-sensitive dyes used in this study. A structural depiction of the model is given in Figure 3, where the mapping of the atoms to coarse-grained beads is indicated; topology parameters are given in the figure caption. The model building procedure and optimization is described in detail in the Materials and Methods section and in the Supporting Information. Where possible, we followed the published standard recipe[35] to construct the basic topology. In the MARTINI model, two to four non-hydrogen atoms are combined into one interaction site, which for Di-4-ASPBS (**1**) leads to a reduction of the number of interaction sites from 31 non-hydrogen atoms (67 atoms including the hydrogen atoms) to 11 beads. Nonstandard problems, such as how to ensure the planarity of the aromatic system, were solved in a way that allowed for a large 40 fs time step in the simulations. We decided to allow the aniline C−N bond, which corresponds to the bond between beads 8 and 9 in Figure 3, to rotate freely despite its partial double bond character because we found that introducing dihedral potentials to control rotation was not compatible with large time steps.

To optimize the coarse-grained model, we constructed a reference atomistic model of Di-4-ASPBS (**1**) within the framework of the GROMOS 53A6 force field, as described in the Supporting Information. To obtain values to which the coarse-grained model could be compared, an atomistic simulation of the dye in water was performed, and a "mapped atomistic" trajectory was produced by combining groups of atoms into coarse-grained beads in accordance with the coarse-grained model (cf. Figure 3). We then compared selected angle and dihedral distributions of the mapped atomistic and coarse-grained models, and iteratively optimized the coarse-grained topology as described in the Materials and Methods section and Supporting Information. This approach is similar to the recently published parametrization of coarse-grained amino acid side chain angles by comparison to angle distributions found in proteins deposited in the Protein Database (PDB).[53]

Validation of the Model. Simulations of the coarse-grained and atomistic models of the dyes were performed to test the agreement between the models and to validate them against experimental data. For this test, we investigated the location of the dye in the membrane and the tilt angle of the chromophore with respect to the membrane normal.

Figure 4 shows the distribution of the position of selected beads of Di-4-ASPBS (**1**) when it is bound to a POPC membrane during a simulation at 323 K. The figure depicts the bead locations both for a 50 ns simulation using the coarse-grained model and for a 45 ns atomistic simulation where the atoms have been mapped onto the coarse-grained structure. Generally, both models agree well with each other. Following from the data, and illustrated also by a snapshot from the atomistic simulation (Figure 4B), the chromophore and the hydrophobic tail of Di-4-ASPBS (**1**) are inserted into the hydrophobic interior of the membrane; the charged pyridinium atom of the chromophore resides within the charged headgroup region of the membrane, and the sulfonate headgroup of the amphiphile is located in the membrane/water interface. These findings are in accord with the interpretation of experimental data on similar styryl-type probes[16,17,54] and a recent computational study.[55] Upon close inspection, we find that the coarse-grained chromophore and tail are located slightly deeper inside the membrane compared to the atomistic simulation. This might be due to a difference in assigning the positive charge in the aromatic ring. In the coarse-grained model, the positive charge is located exclusively at the pyridinium nitrogen, while the charge is distributed over the whole chromophore in the atomistic model (cf. the topologies in the Supporting Information). In addition, the hydrophobic tail of the dye reaches further into the center of the membrane due to the slightly increased length of the coarse-grained model which is a result of retaining the aniline nitrogen as a branching point.

The tilt angle of the chromophore in the membrane with respect to the membrane normal was evaluated for the same atomistic simulation and a coarse-grained simulation with an increased total simulation time of 380 ns to improve convergence. For the evaluation, the chromophore long axis was assumed to run between beads 3 and 8 of the coarse-grained

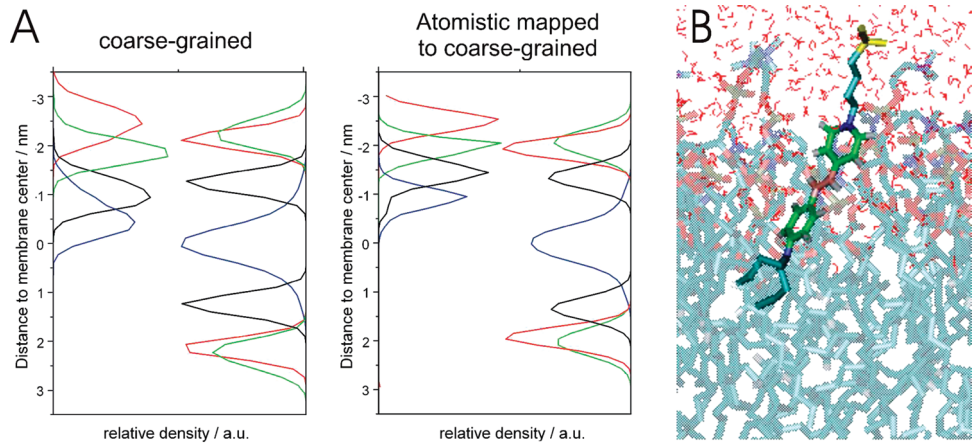

Figure 4. Location of the dye Di-4-ASPBS (**1**) in a membrane of POPC at 323 K. (A) Coarse-grained model (left) and atomistic model mapped to the coarse-grained model (right). In each graph, the relative mass density of selected coarse-grained beads is shown as a function of the distance to the membrane center for Di-4-ASPBS (**1**) (left) and POPC (right). The selected beads for the dye are the sulfonate headgroup (bead 1, red), the pyridinium nitrogen (bead 3, green), the aromatic carbon next to the aniline nitrogen (bead 8, black), and one of the lipophilic tails (bead 10, blue). For POPC, the choline headgroup (red), the phosphatidyl residue (green), and the beads corresponding to the lipid carbons C1−C4 (black) and C12−C16 (blue) are shown. (B) Snapshot of the atomistic simulation of Di-4-ASPBS (**1**) in the POPC membrane. Only one leaflet of the membrane is shown, with lipids depicted in light blue and water molecules in red.

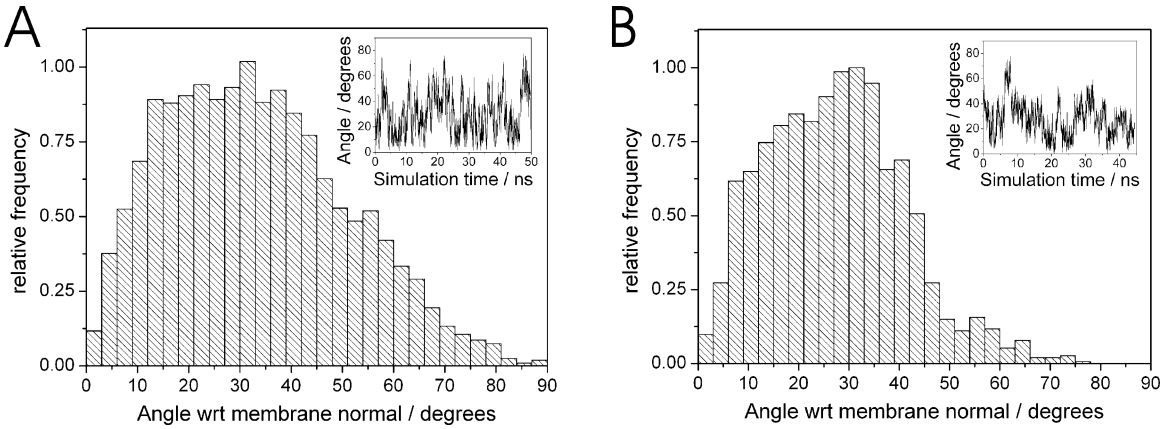

Figure 5. Tilt of the chromophore long axis of Di-4-ASPBS (**1**) between beads 3 and 8 with respect to the membrane normal. Histograms of the angle distributions and plots of the tilt angle over time (insets). (A) Coarse-grained simulation of 380 ns duration. (B) Mapped atomistic simulation of 45 ns duration.

model (cf. Figure 3). Histograms for the coarse-grained model and the atomistic model mapped to the coarse-grained topology are shown in Figure 5. The histograms demonstrate that the chromophore can adopt orientations ranging from aligned (0°) to perpendicular to the membrane normal (90°); mainly, the chromophore is oriented between 10 and 45° with respect to the membrane normal both for the coarse-grained and the atomistic simulations. The remarkably large freedom of the dye to change its tilt angle is in agreement with time-resolved fluorescence anisotropy measurements with the related styryl-type dye RH 421 in a lipid membrane.[20] Describing the motion of the dye around a position parallel to the membrane normal by a "wobbling-in-a-cone" model, Visser et al. found a large cone angle relative to the membrane normal of nearly 50°.[20]

The average angle for the mapped atomistic simulation amounted to $\langle\phi\rangle = 27 \pm 8°$; here and in the following, we use the standard deviation of 5 ns block averages as a measure of the variability of the angle. For the coarse-grained simulation, the average angle amounted to $\langle\phi\rangle = 36 \pm 10°$. Experimental data obtained by fluorescence methods on the similar dye Di-8-ANEPPS in supported POPC membranes on a silicon chip[18] yielded an average inclination of 38°, a value which has been backed up by measurements on black lipid membranes, where an inclination of 36° has been found.[19] Taking into account that the simulation time for the atomistic simulation is not sufficient for the average angle to be converged, the simulations agree well with each other and experimental results.

Dye Models for Di-4-ASPBS Derivates. On the basis of the coarse-grained model of Di-4-ASPBS (**1**), we now constructed models of dye derivatives in order to investigate their behavior in membranes and their binding to membranes. The model construction was performed following the standard MARTINI approach.[35] First, we constructed a series of dyes by varying their tail length. The dyes either contained no lipophilic tail at all (ASPBS, dye **6**), two octyl tails represented by two C1 beads each (Di-8-ASPBS, dye **7**), or two dodecyl tails represented by three C1 beads (Di-12-ASPBS, dye **8**). Further, we built models for the two dye derivative pairs **2** to **5** which have been used for enzyme activated binding, as depicted in Figure 6 (cf. Figure 2). Despite the fact that under experimental conditions[13−15] the phosphate group should be fully deprotonated and therefore doubly negatively charged, we only assigned a single negative charge to the Qa beads, due to the lack of an independent parametrization of doubly charged particles in the MARTINI force field.

Starting structures of the dyes in a lipid membrane were constructed on the basis of Di-4-ASPBS (**1**) in a membrane, and the systems were allowed to equilibrate. We performed long

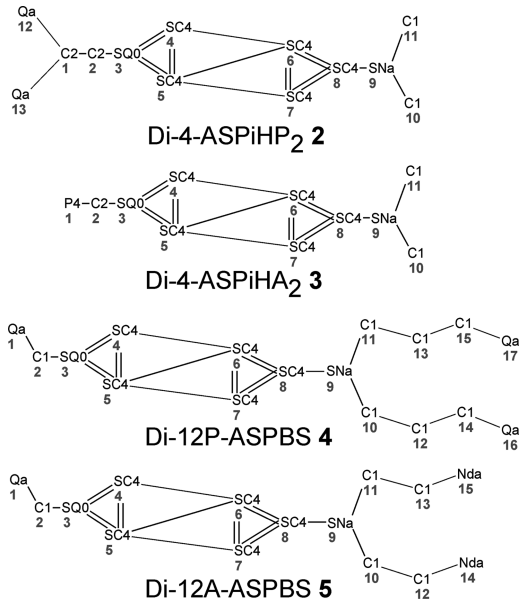

Figure 6. Coarse-grained representation of the voltage-sensitive dyes used in enzyme activated binding (Figure 2). The models are based on the model of Di-4-ASPBS (**1**) (Figure 3). All additional bonds and angles are represented by standard values. All Qa beads are assigned a charge of –1, and the SQ0 beads carry a charge of +1.

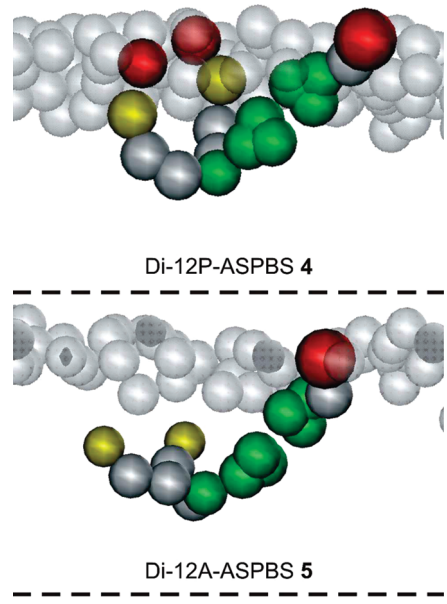

Figure 7. Snapshots of free coarse-grained simulations of Di-12P-ASPBS (**4**) (top) and Di-12A-ASPBS (**5**) (bottom) in a POPC membrane. Of the lipids, only the charged headgroups are shown (transparent gray) and only one leaflet of the membrane, with the dashed line indicating the membrane center. The full coarse-grained representation of the dye molecules is depicted, with the butanol (yellow), alkyl (gray), chromophore (green), and sulfonate/phosphate beads (red), respectively.

coarse-grained simulations of up to 380 ns and investigated the location of the dyes and the chromophore tilt angle in the membrane. We found that the dyes containing a lipophilic tail (Di-8-ASPBS (**7**), Di-12-ASPBS (**8**), Di-4-ASPiHP$_2$ (**2**), Di-4-ASPiHA$_2$ (**3**)) behave analogously to the parent compound Di-4-ASPBS (**1**) in the membrane. For ASPBS (**6**), the lack of a nonpolar tail led to the loss of tight anchoring of the dye tail in the interior of the membrane. This is reflected by an increased average angle of 59 ± 12° with respect to the membrane normal. Interestingly, the average angle decreased with increasing chain length from 36 ± 10° for Di-4-ASPBS (**1**) via 29 ± 8° for Di-8-ASPBS (**7**) to 26 ± 7° for Di-12-ASPBS (**8**). Such a decrease in tilt angle should lead to an increased voltage sensitivity of the dye due to an improved alignment of the chromophore with the membrane normal and a concomitant stronger interaction of the transition dipoles with the electrical field across the membrane. Indeed, it has been observed that long-chain versions of voltage-sensitive dyes tend to exhibit a larger voltage sensitivity than their short-chain analogues, as reported for RH160 and its analogues[56] and for the pair Di-8-ANEPPS/Di-4-ANEPPS.[57] However, assigning this larger voltage sensitivity to an improved orientation in the membrane was difficult so far, because secondary effects like solubility, staining efficiency, interaction with membrane proteins, flip-flop, and internalization can dominate and moreover are also affected by the alkyl chain length.

For the dyes with polar tails, Di-12P-ASPBS (**4**) and Di-12A-ASPBS (**5**), the geometry of binding was changed. We observed a strong preference of the tails for the polar lipid headgroup region and a concomitant backbending of the tails toward the membrane/water interface; this is demonstrated by snapshots of the simulations in Figure 7. Despite this dramatic change in the binding geometry, the average chromophore tilt angle was only slightly increased, amounting to 42 ± 11° for Di-12P-ASPBS (**4**) and 47 ± 10° for Di-12A-ASPBS (**5**). This result sheds light on the previously unknown geometry of binding of these dyes to the lipid membrane.[14,15] In accordance with qualitative fluorescence polarization measurements of the closely related dye Di-10A-ASPBS in giant lipid vesicles,[15] it illustrates why attaching polar groups to the tail of a voltage-sensitive dye need not have strong adverse affects on its chromophore orientation and therefore voltage sensitivity.

Optimizing Conditions for Umbrella Sampling. We now employed umbrella sampling[37] to calculate the potential of mean force of the dyes when pulled through one leaflet of a lipid bilayer. In this method, an additional potential is imposed on a molecule of interest, which constrains it to a defined place along a reaction coordinate. This allows the sampling of phase space along the full reaction coordinate in regions which are not accessible to the molecule by thermal energy alone. In preliminary umbrella sampling simulations, we experienced sampling problems due to the large size and flexibility of the molecules under study. Therefore, we first tested different simulation conditions with Di-4-ASPBS (**1**) for their suitability to obtain reliable results. As the main parameter, we investigated the choice of beads upon which the constraining potential was imposed. To assess convergence, we computed PMFs from the two possible extreme starting conditions: in the "equilibrium" PMF, the dye was positioned in its equilibrium binding position as obtained from a long free simulation; in the "nonequilibrium" simulations, the dye was located in the water phase, or, for the umbrella positions in the membrane interior, bound to the opposite leaflet of the membrane.

We performed umbrella sampling simulations constraining either the polar headgroup (bead 1, Figure 8A) or the center of the molecule (beads 5 and 6, Figure 8B). A comparison of the "equilibrium" (solid lines) and "nonequilibrium" (broken lines) PMFs shows that when the polar headgroup is constrained, the profiles are converged with respect to the flip-flop transition but not at all converged with respect to the transition from water to the membrane (which correlates with the binding free energy). In contrast, when the center of the molecule is constrained, the profiles are much better converged regarding the transition from water to the membrane. Comparing the "equilibrium" simula-

tions (solid lines in Figure 8A and B), the total difference in the PMF regarding the transition from water to the membrane is in good agreement, in contrast to the barrier of the flip-flop transition which is much higher in the case where the polar headgroup is constrained.

The cause for these discrepancies is incomplete sampling, as illustrated in the case of the flip-flop transition. An analysis of the umbrella sampling simulations at the center of the membrane showed that the dye molecule sampled conformations in both leaflets only when the polar headgroup was constrained, while when the center of the molecule was constrained the polar headgroup of the dye remained in one leaflet during the complete simulation time; in that case, the flip-flop transition was not sampled, and the barrier to flip-flop is consequently too small. We tested whether increasing the total simulation time for the umbrella positions close to the center of the membrane (−0.8 to 0 nm) to a total of 480 ns alleviates this problem (Figure 8C). The PMFs do not significantly change in this region when the simulation time is increased.

An analogous problem occurs for the transition from water to the membrane. When the polar headgroup is constrained (Figure 8A), the detachment from the membrane or the integration into it is not well sampled, as judged from an analysis of the umbrella sampling simulations in that region for the different starting conditions. Thus, the apparent absence of a barrier for insertion of the molecule into the membrane is an artifact due to nonoptimal sampling. The situation changes when beads 5 and 6 in the center of the molecule are constrained. In this case, the transition from water to the membrane is quite well sampled irrespective of the starting conditions, and a barrier for insertion becomes apparent (Figure 8B). The agreement between the different extreme starting conditions can be improved even further by increasing the simulation time in the region around the barrier (−3.5 to −2.5 nm) to a total of 480 ns (Figure 8C).

Taking the insights of the test simulations together, we chose the following conditions for further umbrella sampling: (i) The beads that were constrained in the calculations were chosen to be close to the center of the molecule; for the dyes **1**, **2**, **3**, and **6**, this corresponds to beads 5 and 6, while for the long-tailed dyes **4**, **5**, **7**, and **8**, bead 9 was constrained. These choices are required for good sampling of the water/membrane transition but inevitably lead to a nonoptimal sampling of the flip-flop transition; the PMF in the latter region should be regarded as the lower bound of possible values. (ii) To account for the slow convergence of the profiles in the membrane/water interface region, the umbrella positions in these regions were simulated for an additional 400 ns, summing up to a total of 480 ns. (iii) To further improve sampling, the simulations were performed at an elevated temperature (323 K) compared to the temperature at which the experimental binding constants have been obtained (298 K). (iv) The production runs were performed starting from the equilibrium position, because these were found to converge faster to the "final" profile obtained after full simulation. Where necessary, simulations starting from nonequilibrium starting conditions were also performed to assess the convergence of the simulations. Potential of mean force profiles were obtained from the full trajectories, and in order to assess the variability of the results, the first and second halves of all trajectories were also evaluated independently.

PMF for Di-4-ASPBS. The profile resulting from a simulation starting from an equilibrium simulation for Di-4-ASPBS (**1**) is plotted in Figure 9 (solid line), together with the PMFs corresponding to the first and second halves of the trajectory

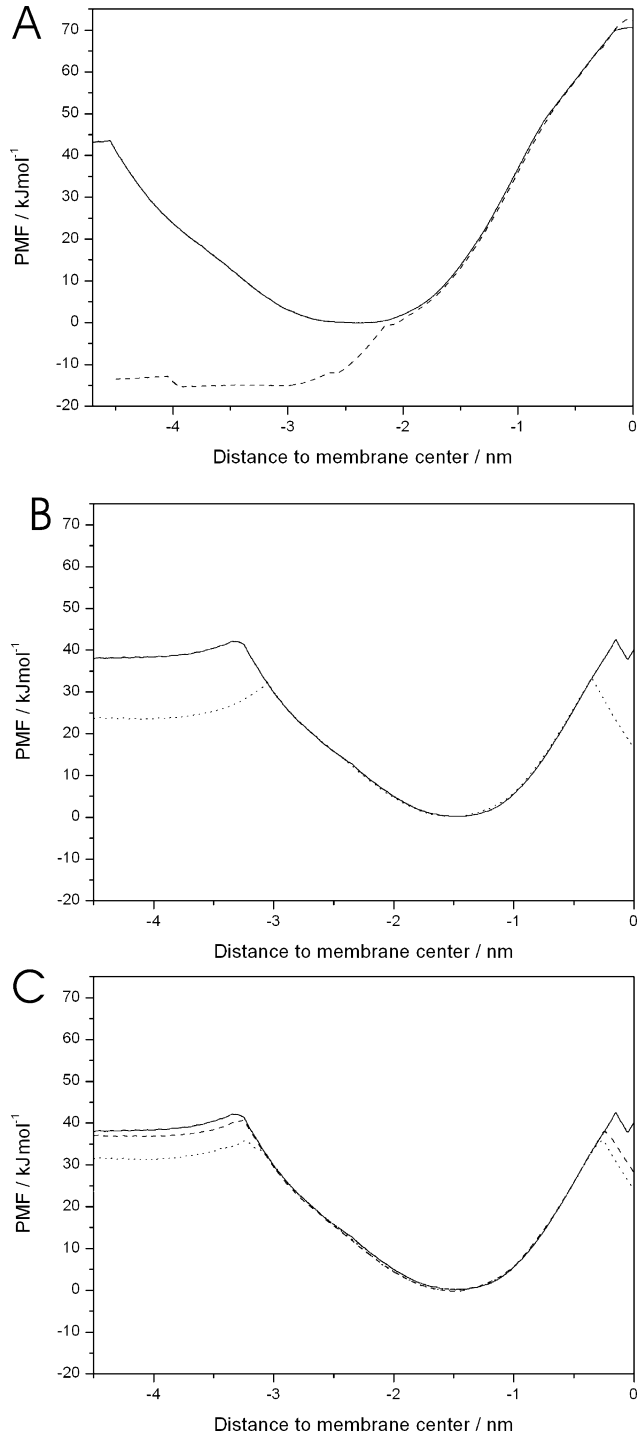

Figure 8. Dependence of the PMF of Di-4-ASPBS (**1**) in a POPC membrane on choice of beads that are constrained, starting conditions, and sampling time. (A and B) PMF profiles from 80 ns simulations with the umbrella potential acting on the headgroup (bead 1, A) or the center (beads 5 and 6, B) of the coarse-grained Di-4-ASPBS (**1**) model. Simulations were started with the dye in its equilibrium position (solid line) as obtained from long free simulations, or from a nonequilibrium position (A, dashed line; B, dotted line) corresponding to the dye being in the other leaflet of the membrane (for positions −1.7 to 0 nm) or in water (−4.5 to −1.7 nm). (C) PMF profiles from the simulation corresponding to part B but with the simulation time increased to a total of 480 ns in the regions of the profile corresponding to the membrane/water interface and the center of the membrane. Shown are independent evaluations of the simulations starting from nonequilibrium positions for the first (dotted line) and second (dashed line) halves of the trajectory, compared to the PMF obtained from the equilibrium simulation (solid line).

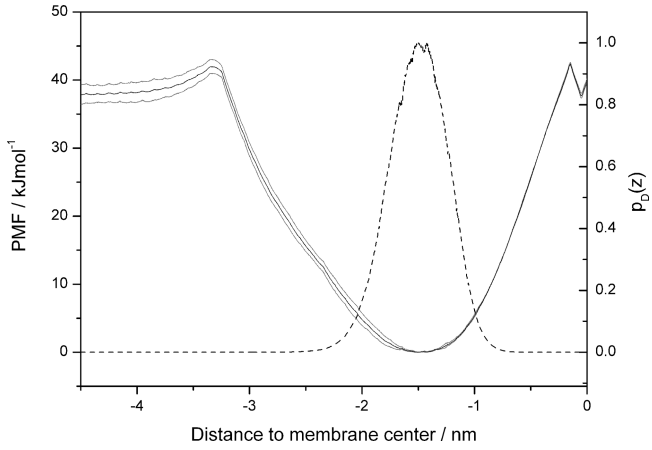

Figure 9. Potential of mean force (PMF) profile and probability distribution $p_D(z)$ for Di-4-ASPBS (**1**) in a POPC membrane. Umbrella sampling calculations on the coarse-grained level were run at 323 K for 80 ns, preceded by a 20 ns equilibration period. For selected parts of the profile, the simulation was continued for a total of 480 ns. The PMF was calculated from either the full (solid black curve) or the respective first and second half of the simulation (gray lines). The corresponding probability distribution $p_D(z)$ is shown as a dotted line. Both the PMF profiles and the probability distributions refer to the relative position of the beads 5 and 6 of the Di-4-ASPBS (**1**) coarse-grained model (that have been constrained during the umbrella sampling simulations) with respect to the center of the membrane.

(gray lines). The figure also contains the probability distribution $p_D(z)$ corresponding to the total PMF (dashed line), illustrating that the bound molecule is confined to the membrane, with a binding width of less than 2 nm. When the dye is pulled from its equilibrium position either out of the membrane or further toward the center, the PMF rises steeply. The profiles resemble the model used by Fromherz and Röcker[12] to describe binding equilibria in terms of an Ostwald coefficient. Their model consists of a plateau value of the free energy in the water phase and a harmonic binding well in the membrane phase. In addition to the features of this model, the PMF profiles exhibit a small barrier for the transition of the dye molecule across the water/membrane interface. The resulting free energy for transfer from water to the membrane calculated by eq 4 is $\Delta G_{PMF,1} = 34.9 \pm 1.2$ kJ mol^{-1}, the height of the barrier against insertion into the membrane is around 5 kJ/mol, and the barrier for flip-flop amounts to around 40 kJ/mol; however, the latter value must be viewed as a lower bound as discussed above, due to the choice of parameters that favor sampling of the transition from water to the membrane interior but do not guarantee sufficient sampling of the flip-flop transition.

Alkyl Chain Length and Binding Free Energy. We now determined the potentials of mean force for dyes **6**−**8** in which the length of the hydrophobic tail was varied. Their PMF profiles are plotted in Figure 10, with the profile for Di-4-ASPBS (**1**) (cf. Figure 9) included for comparison. The free energies of transfer from water to the equilibrium position derived from the PMF profiles $\Delta PMF_{Equ/Wat}$ are collected in Table 1, together with the conversions to the dimension-free binding constant $C_{PMF,Mem/Wat}$ and free energy values ΔG_{PMF} as computed by eqs 3 and 4 (Materials and Methods). We find a nearly linear increase of the binding free energy with chain length, corresponding to 14.0 kJ/mol for each C1 bead if the complete set of data is fitted by linear regression, or 3.5 kJ/mol per methylene group taking into account that each C1 bead represents four methylene groups. The magnitude of the free energy change is close to the transfer free energy of a C1 bead between water and hexadecane (18.0 kJ/mol) against which the C1 bead was parametrized.[35] As expected for the interior of the membrane, the hydrophobic tail therefore experiences a nonpolar environment similar to a bulk hydrocarbon solvent.

For comparison, we may look at experimental data that has been obtained for the dyes Di-2-ASPBS to Di-6-ASPBS.[12] To allow for a comparison, the experimental binding constants need to be converted to a dimensionless binding constant $C_{Mem/Wat}$, as discussed in the Materials and Methods section. The respective binding constants and the free energies of transfer computed from them are given in Table 1 and plotted in Figure 10. The figure illustrates the previous finding[12] that also in experiment there is a linear increase of binding free energy with chain length. The extrapolated experimental binding free energy for the dye without a lipophilic tail ASPBS (**6**) is close to the simulated value; the chromophore and headgroup of Di-4-ASPBS (**1**) are therefore well represented by the coarse-grained model. However, there is a discrepancy between simulation and experiment regarding the increase in binding with alkyl chain length: the experimental increase is considerably smaller and amounts to only 2.4 kJ/mol per methylene group.

To test whether this is due to hydrophobic interactions being generally overestimated by the MARTINI force field, we looked at the membrane binding free energy of linear long-chain alcohols as a second, more simple test case. The binding of alkanols to lipid membranes has been studied experimentally for chain lengths ranging from 1 to 9.[58] It was found that the binding free energy increases linearly with chain length, with an average slope of 3.8 kJ mol^{-1} per methylene group. To check whether these results could be reproduced by simulation, we built coarse-grained models representing butanol, octanol, and dodecanol and computed PMF profiles of these models in a lipid membrane (see Figure 1 in the Supporting Information). We found a linear increase in binding free energy of 3.5 kJ mol^{-1} per methylene group, in very good agreement with the experimental data. Not only the relative increase per methylene group but also the absolute binding free energies are in good agreement with experiment (see Figure 1 in the Supporting Information). The discrepancy between simulation and experiment for the binding of the voltage-sensitive dyes is therefore not due to a general overestimation of hydrophobic interactions in the MARTINI force field. It is striking that the relative increase in binding free energy per methylene group as obtained by simulation is the same for the linear alcohols and the amphiphilic dyes. Possibly, secondary effects exist that reduce the experimental binding free energy for amphiphiles containing two lipophilic chains but that are not well reproduced by the coarse-grained model, for example, a mutual shielding of the hydrophobic tails in water. On the other hand, it may also be that the experimental binding constants are influenced by interactions between the dye molecules in water and therefore do not reflect the true binding free energy of a single dye molecule that is the result of the umbrella sampling calculations. The tendency of styryl-type dyes to form aggregates in aqueous solution has, for example, been documented for the dye RH 421.[21] Further studies are required to clarify this point.

Polar Groups and Binding Free Energy. The potentials of mean force for the amphiphilic dyes used in enzyme activated binding are plotted in Figure 11. The free energies of transfer derived from the PMF profiles by eq 4 are collected in Table 1, together with a summary of the experimental numbers and respective conversions to free energy values. The simulated binding free energies are larger than the experimental values, an effect which increases with increasing chain length; this can be assigned to the overestimated increase per methylene group

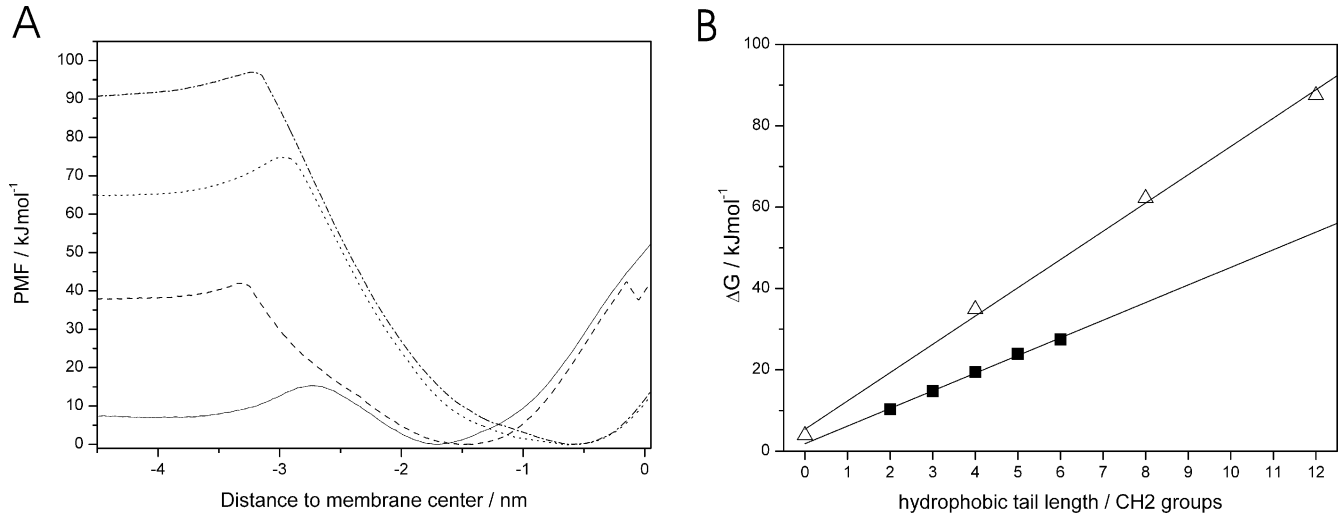

Figure 10. Potentials of mean force and binding free energies for dyes with varying hydrophobic tail lengths in a POPC membrane. (A) PMF profiles. Plotted are curves for the dyes ASPBS (**6**) (solid line), Di-4-ASPBS (**1**) (dashed line), Di-8-ASPBS (**7**) (dotted line), and Di-12-ASPBS (**8**) (dashed−dotted line). The profiles correspond to 80 ns umbrella sampling simulations except in the region which corresponds to the membrane/water interface which was further simulated to a total of 480 ns. (B) Free energy and hydrophobic tail chain length. Plotted is the free energy of binding ΔG_{PMF} for the dyes **1**, **6**, **7**, and **8** obtained by the PMF calculations (triangles), and for comparison experimental data ΔG_{EXP} for the dyes Di-2-ASPBS to Di-6-ASPBS (squares).[12] The conversion of experimental binding constants and PMF values to free energies is described in the Materials and Methods section.

TABLE 1: Overview of Binding Data[a]

	K_{EXP}	$\Delta PMF_{Equ/Wat}$	$C_{EXP,Mem/Wat}$	$C_{PMF,Mem/Wat}$	ΔG_{EXP}	ΔG_{PMF}
ASPBS (**6**)		−7.2		4.3		−3.9
Di-4-ASPBS (**1**)	7500	−37.8	9.7×10^3	4.4×10^5	−22.7	−34.9
Di-8-ASPBS (**7**)		−65.0		1.2×10^{10}		−62.2
Di-12-ASPBS (**8**)		−90.7		1.4×10^{14}		−87.5
Di-4-ASPBSiHP$_2$ (**2**)	700	−31.5	9.1×10^2	2.9×10^4	−16.9	−27.6
Di-4-ASPBSiHA$_2$ (**3**)	15600	−40.2	2.0×10^4	8.7×10^5	−24.6	−36.7
Di-12P-ASPBS (**4**)	2100	−48.9	2.7×10^3	2.3×10^7	−19.6	−45.5
Di-12A-ASPBS (**5**)	3 000 000	−55.2	3.9×10^6	2.7×10^8	−37.6	−52.1

[a] The experimental binding constants K_{EXP} (with units of M^{-1}) are taken from refs 13−15. $\Delta PMF_{Equ/Wat}$ corresponds to the difference in free energy in kJ mol^{-1} between the dye in water and the dye in its equilibrium position. The experimental dimension-free binding constant $C_{EXP,Mem/Wat}$ and the corresponding free energy ΔG_{EXP} (in kJ mol^{-1}) were computed from K_{EXP} using eqs 7 and 8 (see Materials and Methods). The simulated binding constant $C_{PMF,Mem/Wat}$ and the corresponding free energy of binding ΔG_{PMF} (in kJ mol^{-1}) were obtained from the PMF profiles using eqs 3 and 4.

as discussed in the preceding section. If we look at the *relative* changes in free energy for the dyes modified at the headgroup, i.e., Di-4-ASPBS (**1**), Di-4-ASPiHP$_2$ (**2**), and Di-4-ASPiHA$_2$ (**3**), we find good agreement with the experimental data (Table 3). While the binding free energies for Di-4-ASPBS (**1**) and Di-4-ASPiHA$_2$ (**3**) are nearly the same, the phosphorylated dye Di-4-ASPiHP$_2$ (**2**) exhibits a binding free energy which is reduced relative to Di-4-ASPiHA$_2$ (**3**) by $\Delta G_{2-3}^{umbrella} = 9.1$ kJ mol^{-1}, compared to the experimental value of $\Delta G_{2-3}^{exp} = 7.7$ kJ mol^{-1}. For the dye phosphorylated at the tail Di-12P-ASPBS (**4**), compared to the extrapolated binding free energy (Figure 10A) of Di-12-ASPBS (**8**), we find rather good agreement for the relative change in free energy. Introducing a phosphate group at the tail of the dye reduced the binding free energy by $\Delta G_{D12-D12P}^{umbrella} = 42.0$ kJ mol^{-1}, as compared to the extrapolated experimental difference of $\Delta G_{D12-D12P}^{exp} \approx 34$ kJ mol^{-1}. Both in experiment and simulation, there is a more than 3-fold difference in the impact on binding free energy that is exerted by a phosphate group attached to the lipophilic tail as compared to when it is attached to the polar headgroup. The simulations also provide insights into why this difference exists: When the phosphate groups are attached to the polar headgroup of the dye, the binding mode of the dye and the nonpolar interactions remain nearly undisturbed; the phosphate groups are in an environment that is already quite polar. When the phosphate groups are attached to the lipophilic tails, the binding mode is affected drastically. This is because it is energetically unfavorable for both the phosphate group to be dragged into the hydrophobic interior of the membrane and the hydrophobic alkyl chains to be removed from it. The geometry of binding reflects this balance, with the phosphate group being fixed at a position of around 2 nm away from the membrane center, and the lipophilic tail being forced to backbend toward the membrane/water interface (Figure 7).

If we compare the binding free energy of the alcohol-containing dye Di-12A-ASPBS (**5**) with Di-12-ASPBS (**8**) and Di-12P-ASPBS (**4**), we find that the impact of introducing a hydroxyl group at the tail is significantly overestimated by the simulations: We obtain a difference of $\Delta G_{D12-D12A}^{umbrella} = 35.4$ kJ mol^{-1}, while the extrapolated experimental difference amounts to only $\Delta G_{D12-D12A}^{exp} = 16.3$ kJ mol^{-1}. This discrepancy is not due to insufficient sampling in the simulations, as indicated by the very similar PMF profile obtained with nonequilibrium starting conditions (Figure 11, dotted lines). Rather, it is due to the repulsion of the Nda particle—which represents butanol at the dye tail—from the hydrophobic interior of the membrane

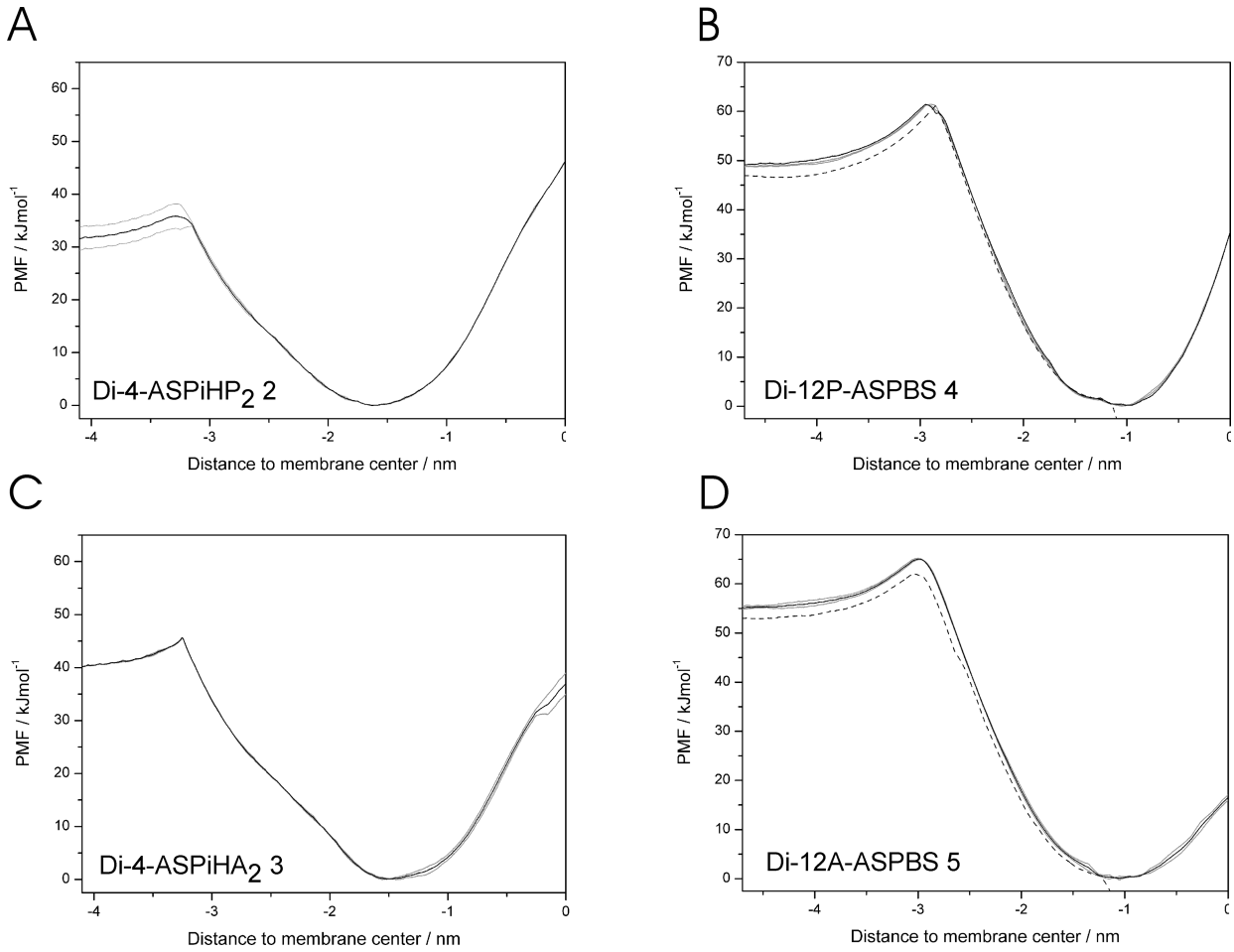

Figure 11. Potentials of mean force for dyes used in enzyme activated binding (cf. Figure 2) in a POPC membrane. The precursor amphiphiles contain polar phosphoric acid ester groups at the head (A: Di-4-ASPiHP$_2$ (**2**)) or tail (B: Di-12P-ASPBS (**4**)). The corresponding activated dyes contain hydroxyl groups at the head (C: Di-4-ASPiHA$_2$ (**3**)) or tail (D: Di-12A-ASPBS (**5**)), respectively. The PMFs were obtained with coarse-grained models built by the standard recipe (cf. the Supporting Information for PMFs of alternative representations). They correspond to 80 ns umbrella sampling simulations except in the region which corresponds to the membrane/water interface which was further simulated to a total of 480 ns. Shown are the PMF profiles corresponding to the full simulation time (solid line) and to the respective first and second halves of the simulation time (gray lines). For the dyes Di-12P-ASPBS (**4**) (C) and Di-12A-ASPBS (**5**) (D), the potential of mean force obtained from nonequilibrium starting conditions is also shown (dashed lines).

being too strong. Following the MARTINI standard recipe to represent the dodecanol tail of Di-12A-ASPBS (**5**) therefore leads to only qualitatively correct results, with binding strength decreasing in the order Di-12-ASPBS (**8**) > Di-12A-ASPBS (**5**) > Di-12P-ASPBS (**4**). However, the quantitative agreement was not sufficient to employ this method for the design of optimized amphiphile precursors which could be used for the enzyme induced staining of membranes (Figure 2). In contrast to experiment, the theoretical difference in binding between Di-12P-ASPBS (**4**) and Di-12A-ASPBS (**5**) is lower than the difference between Di-4-ASPiHP$_2$ (**2**) and Di-4-ASPiHA$_2$ (**3**) (Table 3). Because finding a computational method for this purpose was one of the original motivations for us to conduct the presented work, we exploited the flexibility of the MARTINI force field to devise a different strategy to represent dyes containing hydroxyl groups (Di-12A-ASPBS (**5**) and Di-4-ASPiHA$_2$ (**3**)) as described in the following section.

Alternative Model for Hydroxyl Groups. In this approach, the hydroxyl group is introduced analogously to the phosphate group as a separate bead; this has the decisive advantage that the basic structure remains the same for the hydroxyl- and the phosphoric acid ester-containing dye. To account for the fact that the hydroxyl group actually only represents one non-hydrogen atom, the bond length to its connecting neighbor was reduced to 0.37 nm. To represent the hydroxyl group, we tried two bead types of intermediate polarity, P3 and P2 (cf. Figure 2 in the Supporting Information for topologies). These display a transfer free energy between water and hexadecane of $\Delta G_{HW}^{P3} = 21$ kJ mol^{-1} and $\Delta G_{HW}^{P2} = 17$ kJ mol^{-1},[35] values which are slightly smaller than the difference between the Nda and C1 beads[35] (which would correspond to the transfer of a hydroxyl group) which amounts to $\Delta\Delta G_{HW}^{C1-Nda} = 25$ kJ mol^{-1}. We

TABLE 2: Binding Data Obtained by Simulation for Alternative Dye Topologies[a]

	$\Delta PMF_{Equ/Wat}$	$C_{PMF,Mem/Wat}$	ΔG_{PMF}
Di-4-ASPiHA$_2$ (**3**)	−40.2	8.7×10^5	−36.7
Di-4-ASPiHA$_2$/P3 bead	−41.5	1.8×10^6	−38.6
Di-4-ASPiHA$_2$/P2 bead	−43.4	2.9×10^6	−40.0
Di-12A-ASPBS (**5**)	−55.2	2.7×10^8	−52.1
Di-12A-ASPBS/P3 bead	−63.6	6.2×10^9	−60.5
Di-12A-ASPBS/P2 bead	−74.0	3.6×10^{11}	−71.4

[a] The simulated dimension-free binding constant $C_{PMF,Mem/Wat}$ and the corresponding free energy of binding ΔG_{PMF} (in kJ mol^{-1}) were obtained from the PMF profiles using eqs 3 and 4 (see Materials and Methods).

TABLE 3: Binding Free Energy Differences (in kJ mol^{-1}) in Experiment and Simulation[a]

	$\Delta(\Delta G_{EXP})$	$\Delta(\Delta G_{PMF}^{standard})$	$\Delta(\Delta G_{PMF}^{P3})$	$\Delta(\Delta G_{PMF}^{P2})$
Di-4-ASPiHA$_2$ (**3**)/Di-4-ASPBS (**1**)	−1.8	−1.9	−3.8	−5.1
Di-4-ASPiHP$_2$ (**2**)/Di-4-ASPiHA$_2$ (**3**)	+7.7	+9.1	+11.1	+12.4
Di-12P-ASPBS (**4**)/Di-12-ASPBS (**8**)	+34.3	+42.0	+42.0	+42.0
Di-12A-ASPBS (**5**)/Di-12-ASPBS (**8**)	+16.3	+35.4	+27.0	+16.1
Di-12P-ASPBS (**4**)/Di-12A-ASPBS (**5**)	+18.0	+6.6	+15.0	+25.9

[a] The values obtained by simulation refer to the different approaches used to represent the hydroxyl group in the dyes, i.e., as part of a bead ("standard") or as a separate P3 or P2 bead (see text).

performed simulations for the alternative models of Di-4-ASPiHA$_2$ (**3**) and Di-12A-ASPBS (**5**) with both bead types. The PMF profiles are given in Figure 3 of the Supporting Information. The corresponding PMF and binding free energy values are given in Table 2, and the differences in binding free energy between selected dyes are shown in Table 3. An inspection of the data shows that, with decreasing polarity of the bead representing the hydroxyl group, the binding free energy for Di-4-ASPiHA$_2$ (**3**) increases only slightly, while the binding of Di-12A-ASPBS (**5**) increases quite strongly, compared to the models of the dyes that were constructed by the standard approach. This behavior is as expected from the locations of the beads at the head or the tail of the dye. If we look at the resulting differences in binding between phosphoric acid ester-containing precursor dyes and their hydroxyl-containing counterparts (Table 3), we find that now—in accord with experiment—the difference between Di-12P-ASPBS (**4**) and Di-12A-ASPBS (**5**) is larger than that between Di-4-ASPiHP$_2$ (**2**) and Di-4-ASPiHA$_2$ (**3**). The difference is more pronounced when the hydroxyl group is represented by the less polar P2 bead. While also when we use the strategy to represent the alcohol group as a separate bead the agreement between experiment and simulations is only semiquantitative (Table 3), we do now find a clear difference in the impact on binding depending on where we introduce polar alcohol groups in the amphiphile. This should be a sufficient basis to utilize coarse-grained molecular dynamics simulations for improving the design of amphiphile precursors that can be used in the enzymatically activated binding of amphiphiles to membranes.

Conclusion

We have performed molecular dynamics simulations of styryl-type voltage-sensitive dyes in a biomembrane on the atomistic and coarse-grained level. The study on the one hand shows that styryl-type voltage-sensitive fluorescent dyes are interesting model amphiphiles. Due to the wealth of high-quality biophysical data available, various aspects of the molecular behavior of a dye in a membrane observed in simulations can be compared to macroscopic experimental data. By simulation, we have obtained new insights into the molecular behavior of these amphiphiles in lipid membranes, some of which should be generalizable to other amphiphiles and lipid-interacting molecular probes. The main results of the simulations are that (i) the chromophore tilt that has been determined in biophysical experiments[18,19] is the average over orientations ranging from aligned to perpendicular to the membrane normal. In line with experimental observations,[20] the simulations illustrate that the dye chromophore is remarkably free to change its orientation in the membrane; (ii) the average tilt of the chromophore is decreased with increasing lipophilic chain length, which should lead to an increased voltage sensitivity and could explain trends that have been observed experimentally;[56,57] (iii) attaching polar groups to the long lipophilic chains of an amphiphilic probe affects the chromophore orientation only weakly, because the hydrophobic chains still anchor the chromophore as far as possible in the membrane interior, even though the polar groups reside at the membrane/water interface; and (iv) the linear increase in binding free energy with increasing lipophilic chain length that has been observed experimentally for chain lengths of up to six methylene groups[12] continues at least up to dodecyl chains according to the simulations; this is of interest because very large binding constants as they would be exhibited by very long-tailed amphiphiles are difficult to access by experiment.

On the other hand, the work represents a thorough analysis of the utility of the MARTINI coarse-grained force field in describing the behavior of amphiphiles in membranes and rapidly estimating the free energy of membrane binding for large, complex molecules. To this end, we have illustrated a viable approach starting from the construction and validation of a coarse-grained model of an amphiphile to performing umbrella sampling calculations under optimized conditions. We have shown that atomistic and coarse-grained simulations agree well with each other and experimental data regarding the location and tilt of voltage-sensitive dyes in lipid membranes. Regarding the free energy of membrane binding, aspects like the increase in binding with increasing lipophilic tail chain length and the differential impact of introducing polar phosphoric acid ester groups at the head or tail of these amphiphiles were semiquantitatively reproduced by the coarse-grained model using a standard recipe for model building. Regarding the introduction of hydroxyl groups, a standard representation only brought qualitatively correct results, which could however be improved by an alternative model building strategy. The latter example showed that minor changes in the molecule representation can have a large impact on binding free energy, and that absolute binding free energies obtained by coarse-grained simulation should be interpreted with care. The study highlighted a discrepancy between simulation and experiment, namely, an overestimation of the free energy increase with increasing chain length of the voltage-sensitive dyes; the underlying reasons for this discrepancy are not clear, but it was shown to not be due to a general overestimation of hydrophobic interactions by the MARTINI force field, because the binding free energies of alkanols of varying chain length obtained from simulation were in good agreement with experiment. Further studies, eventually also using other coarse-grained and fine-grained force fields, are required to clarify this issue.

A major advantage of free energy calculation via molecular dynamics simulations as compared to fragment-based approaches of partition coefficient estimation is that only molecular dynamics simulations are able to take the anisotropy of binding to a membrane into account, without requiring prior knowledge of the position and orientation of the molecule. The voltage-sensitive dyes studied in this work are an extreme test case for the different impact of polar groups on binding depending on their position in the amphiphile, and we show that the MARTINI

coarse-grained model is able to reproduce this difference. Importantly, it delivers binding free energy estimates at a fraction of the computational cost that atomistic simulations would require. Thus, binding free energy calculations with the aid of coarse-grained molecular dynamics simulations are at the same time fast and yet still accurate enough to be a useful computational tool in studying and optimizing membrane-interacting molecules. A direct application of this work is the general design and optimization of amphiphiles that can be enzymatically induced to bind to membranes. More generally, coarse-grained molecular dynamics simulations promise to be useful for the study and optimization of any membrane-interacting molecule, particularly for optimizing biophysical probes, or for adjusting the membrane binding and permeation of pharmaceutical compounds.

Acknowledgment. We thank Prof. Dr. Peter Fromherz for insightful discussions, Dr. Durba Sengupta and Dr. Jelger Risselada for technical advice, and Prof. Dr. Peter Tieleman and his group for providing scripts for umbrella sampling calculations. The initial phase of this work was supported by a postdoctoral grant awarded to M.J.H. from the German Academic Exchange Service (DAAD). Further, M.J.H. gratefully acknowledges support by Prof. Dr. Kai Johnsson.

Supporting Information Available: The Supporting Information contains (1) the atomistic topology of Di-4-ASPBS (**1**) and POPC lipid, (2) tables containing the comparison between selected angle and dihedral distributions of the coarse-grained and of the mapped atomistic simulations used for fine-tuning the coarse-grained model, (3) PMF profiles and experimental data for the binding of alkanols to a POPC membrane, and (4) the topologies and PMF profiles of the alternative representations of the dyes **3** and **5**. This material is available free of charge via the Internet at http://pubs.acs.org.

References and Notes

(1) Cohen, L. B.; Salzberg, B. M.; Grinvald, A. *Annu. Rev. Neurosci.* **1978**, *1*, 171.
(2) Fluhler, E.; Burnham, V. G.; Loew, L. M. *Biochemistry* **1985**, *24*, 5749.
(3) Grinvald, A.; Hildesheim, R. *Nat. Rev. Neurosci.* **2004**, *5*, 874.
(4) Hübener, G.; Lambacher, A.; Fromherz, P. *J. Phys. Chem. B* **2003**, *107*, 7896.
(5) Kuhn, B.; Fromherz, P. *J. Phys. Chem. B* **2003**, *107*, 7903.
(6) Bedlack, R. S., Jr.; Wei, M.; Loew, L. M. *Neuron* **1992**, *9*, 393.
(7) Gross, E.; Bedlack, R. S., Jr.; Loew, L. M. *Biophys. J.* **1994**, *67*, 208.
(8) Buhler, R.; Sturmer, W.; Apell, H. J.; Lauger, P. *J. Membr. Biol.* **1991**, *121*, 141.
(9) Betz, W. J.; Bewick, G. S. *Science* **1992**, *255*, 200.
(10) Betz, W. J.; Mao, F.; Smith, C. B. *Curr. Opin. Neurobiol.* **1996**, *6*, 365.
(11) Brumback, A. C.; Lieber, J. L.; Angleson, J. K.; Betz, W. J. *Methods* **2004**, *33*, 287.
(12) Fromherz, P.; Röcker, C. *Ber. Bunsen-Ges. Phys. Chem.* **1994**, *98*, 128.
(13) Hinner, M. J.; Hübener, G.; Fromherz, P. *J. Phys. Chem. B* **2004**, *108*, 2445.
(14) Hinner, M. J.; Hübener, G.; Fromherz, P. *ChemBioChem* **2006**, *7*, 495.
(15) Hinner, M. J. Genetically Targeted Staining of Cells with Voltage Sensitive Dyes using an Ecto-Enzyme. Ph.D. Thesis, Technische Universität München, 2005.
(16) Pevzner, E.; Ehrenberg, B.; Loew, L. M. *Spectrosc. Lett.* **1993**, *26*, 1181.
(17) Schote, U.; Seelig, J. *Biochim. Biophys. Acta* **1998**, *1415*, 135.
(18) Lambacher, A.; Fromherz, P. *J. Phys. Chem. B* **2001**, *105*, 343.
(19) Ries, R. S.; Choi, H.; Blunck, R.; Bezanilla, F.; Heath, J. R. *J. Phys. Chem. B* **2004**, *108*, 16040.
(20) Visser, N. V.; Vanhoek, A.; Visser, A.; Frank, J.; Apell, H. J.; Clarke, R. J. *Biochemistry* **1995**, *34*, 11777.
(21) Zouni, A.; Clarke, R. J.; Holzwarth, J. F. *J. Phys. Chem.* **1994**, *98*, 1732.
(22) MacCallum, J. L.; Tieleman, D. P. Interactions between small molecules and lipid bilayers. In *Curr. Top. Membr.*; Feller, S. E., Ed.; Elsevier: 2008; Vol. 60, pp 227−256.
(23) Marrink, S. J.; Berendsen, H. J. C. *J. Phys. Chem.* **1994**, *98*, 4155.
(24) MacCallum, J. L.; Tieleman, D. P. *J. Am. Chem. Soc.* **2006**, *128*, 125.
(25) Ulander, J.; Haymet, A. D. J. *Biophys. J.* **2003**, *85*, 3475.
(26) Marrink, S. J.; Berendsen, H. J. C. *J. Phys. Chem.* **1996**, *100*, 16729.
(27) Bemporad, D.; Luttmann, C.; Essex, J. W. *Biophys. J.* **2004**, *87*, 1.
(28) MacCallum, J. L.; Bennett, W. F.; Tieleman, D. P. *J. Gen. Physiol.* **2007**, *129*, 371.
(29) Tieleman, D. P.; Marrink, S. J. *J. Am. Chem. Soc.* **2006**, *128*, 12462.
(30) Marrink, S. J.; de Vries, A. H.; Harroun, T. A.; Katsaras, J.; Wassall, S. R. *J. Am. Chem. Soc.* **2008**, *130*, 10.
(31) Bennett, W. F.; MacCallum, J. L.; Hinner, M. J.; Marrink, S. J.; Tieleman, D. P. *J. Am. Chem. Soc.* **2009**, *131*, 12714.
(32) Voth, G. A. *Coarse-Graining of Condensed Phase and Biomolecular Systems*, 1st ed.; CRC Press: 2009.
(33) Muller, M.; Katsov, K.; Schick, M. *Phys. Rep.-Rev. Sec. Phys. Lett.* **2006**, *434*, 113.
(34) Venturoli, M.; Sperotto, M. M.; Kranenburg, M.; Smit, B. *Phys. Rep.-Rev. Sec. Phys. Lett.* **2006**, *437*, 1.
(35) Marrink, S. J.; Risselada, H. J.; Yefimov, S.; Tieleman, D. P.; de Vries, A. H. *J. Phys. Chem. B* **2007**, *111*, 7812.
(36) Oostenbrink, C.; Villa, A.; Mark, A. E.; Van Gunsteren, W. F. *J. Comput. Chem.* **2004**, *25*, 1656.
(37) Torrie, G. M.; Valleau, J. P. *J. Comput. Phys.* **1977**, *23*, 187.
(38) Van der Spoel, D.; Lindahl, E.; Hess, B.; Groenhof, G.; Mark, A. E.; Berendsen, H. J. C. *J. Comput. Chem.* **2005**, *26*, 1701.
(39) http://www.gromacs.org/.
(40) Van Gunsteren, W. F.; Billeter, S. R.; Eising, A. A.; Hünenberger, P. H.; Krüger, P.; Mark, A. E.; Scott, W. R. P.; Tironi, I. G. *Biomolecular Simulation: The GROMOS96 Manual and User Guide*; Verlag der Fachvereine Hochschulverlag AG an der ETH Zurich: Zürich, 1996.
(41) Thole, B. T.; Van Duijnen, P. T. *Theor. Chim. Acta* **1983**, *63*, 209.
(42) GAMESS-UK is a package of ab initio programs. See: http://www.cfs.dl.ac.uk/gamess-uk/index.shtml. Guest, M. F.; Bush, I. J.; Van Dam, H. J. J.; Sherwood, P.; Thomas, J. M. H.; Van Lenthe, J. H.; Havenith, R. W. A.; Kendrick, J. *Mol. Phys.* **2005**, *103*, 719.
(43) The POPC topology used in this work represents a stage in the development of a GROMOS 53A6 lipid library with modified parameters that reproduce the phase transition behavior of a wide range of lipids.
(44) Berendsen, H. J. C.; Postma, J. P. M.; Van Gunsteren, W. F.; Hermans, J. In *Intermolecular Forces*; Pullman, B., Ed.; D. Reidel Publishing Company: Dordrecht, The Netherlands, 1981; pp 331−342.
(45) Hess, B.; Bekker, H.; Berendsen, H. J. C.; Fraaije, J. G. E. M. *J. Comput. Chem.* **1997**, *18*, 1463.
(46) Miyamoto, S.; Kollman, P. A. *J. Comput. Chem.* **1992**, *13*, 952.
(47) Van Gunsteren, W. F.; Berendsen, H. J. C. *Angew. Chem., Int. Ed. Engl.* **1990**, *29*, 992.
(48) Tironi, I. G.; Sperb, R.; Smith, P. E.; Van Gunsteren, W. F. *J. Chem. Phys.* **1995**, *102*, 5451.
(49) Berendsen, H. J. C.; Postma, J. P. M.; Van Gunsteren, W. F.; Dinola, A.; Haak, J. R. *J. Chem. Phys.* **1984**, *81*, 3684.
(50) Marrink, S. J.; de Vries, A. H.; Mark, A. E. *J. Phys. Chem. B* **2004**, *108*, 750.
(51) Kumar, S.; Bouzida, D.; Swendsen, R. H.; Kollman, P. A.; Rosenberg, J. M. *J. Comput. Chem.* **1992**, *13*, 1011.
(52) Lasch, J. *Biochim. Biophys. Acta* **1995**, *1241*, 269.
(53) Monticelli, L.; Kandasamy, S. K.; Periole, X.; Larson, R. G.; Tieleman, D. P.; Marrink, S. J. *J. Chem. Theory Comput.* **2008**, *4*, 819.
(54) Bammel, B. P.; Hamilton, D. D.; Haugland, R. P.; Hopkins, H. P.; Schuette, J.; Szalecki, W.; Smith, J. C. *Biochim. Biophys. Acta* **1990**, *1024*, 61.
(55) Rusu, C. F.; Lanig, H.; Othersen, O. G.; Kryschi, C.; Clark, T. *J. Phys. Chem. B* **2008**, *112*, 2445.
(56) Grinvald, A.; Hildesheim, R.; Farber, I. C.; Anglister, L. *Biophys. J.* **1982**, *39*, 301.
(57) Rohr, S.; Salzberg, B. M. *Biophys. J.* **1994**, *67*, 1301.
(58) Rowe, E. S.; Zhang, F.; Leung, T. W.; Parr, J. S.; Guy, P. T. *Biochemistry* **1998**, *37*, 2430.

JP907981Y